ACS APPLIED BIO MATERIALS

www.acsabm.org
Article

Gold Nanoparticles Combine with Radiation Therapy to Drive Immunogenic Macrophage Reprogramming

Shalini Iyer,* Tijani Tabarrant, Benjamin Ledoux, Carine Michiels, and Anne-Catherine Heuskin

Cite This: https://doi.org/10.1021/acsabm.6c00342

ABSTRACT: Heavy-metal-based nano-objects have been recently shown to act as radiosensitizers. One possible underlying mechanism causing this effect is the amplification of reactive oxygen species (ROS) production upon irradiation. This reaction could be utilized to improve radiotherapy by repolarizing M2 anti-inflammatory macrophages, which typically constitute the majority of the tumor-associated macrophage population, to the M1 pro-inflammatory phenotype that induces anti-cancer responses, as ROS upregulation has been associated with M1 polarization. This study employs gold nanoparticles (AuNPs) of sizes of 15 or 50 nm, coated with polyvinylpyrrolidone (PVP) or polyethylene glycol. These AuNPs upregulated M1 gene expression and favored the polarization effect of 5 Gy and 10 Gy X-ray irradiation but not of 5 or 10 Gy proton irradiation. Furthermore, 50 nm AuNPs coated with PVP reduced the survival of M2 co-cultured with pancreatic cancer cells, used alone or in combination with 5 Gy X-rays. The findings confirm that AuNPs combined with X-ray radiotherapy can repolarize TAMs to become more M1-like and cytotoxic to pancreatic cancer cells. This work presents an efficient and easy-to-manufacture technique to improve radiotherapy efficacy in solid cancers like pancreatic cancer.

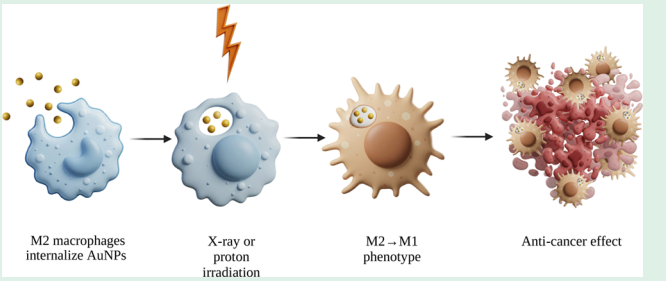

KEYWORDS: *gold nanoparticles, radiotherapy, macrophages, pancreatic cancer, ROS, proton radiation, X-ray radiation*

1. INTRODUCTION

Cancer is a disease that we have been battling for millennia; however, it is still a leading cause of death globally, with nearly 20 million incidences in 2022, of which 50% of the patients generally require radiotherapy.[1,2] Conventional radiotherapy in clinics uses X-ray beams to induce DNA damage and generate intracellular reactive oxygen species (ROS) by breaking down water molecules, further damaging the organelles and disrupting cellular functioning.[3] It aims to induce cell death and trigger an anti-cancer immune response by releasing immunogenic signals, therefore making stubborn tumors vulnerable to treatment, especially when combined with chemotherapy or immunotherapy.[3] Proton therapy, the use of proton beams for cancer treatment, is gaining traction as a potential replacement for X-ray radiotherapy owing to its higher precision in targeting the tumor volume while minimizing the radiation exposure of the nearby healthy tissues, consequently reducing radiation-induced secondary tumors and the side effects caused by radiation toxicity.[4] This is because of the property of a proton beam to retain most of its energy till the beam reaches the end of its path, where it deposits the entire energy at the Bragg peak. This behavior is clinically manipulated to specifically target the tumor.[5]

Macrophages are phagocytic immune cells that infiltrate tumors.[6] The immunological characteristics of mature macrophages can be described as a spectrum of phenotypes, the two ends being pro-inflammatory M1 macrophages and anti-inflammatory M2 macrophages.[6] While M1 macrophages recognize and clear damaged cells in normal physiological conditions and early developmental stages of a tumor, well-developed tumors harbor M2 macrophages known as tumor-associated macrophages (TAMs), which create an immunosuppressive microenvironment.[7] Despite the improvement in cancer detection and therapy, pancreatic cancer still has a low 5-year survival rate of 5–15% because of late detection and infiltration by a large M2 population, leading to the establishment of metastases at the time of detection, hence resulting in difficulty in treatment.[8,9] The presence of a large TAM population has been established to result in a bad prognosis in cancer, and this is quite often the case in pancreatic cancer, where the TAMs sustain pro-tumoral behaviors like epithelial-to-mesenchymal transition, chronic inflammation, invasion, migration, stemness, and resistance to therapy, leading to very low patient survival rates.[9−11]

Received: February 19, 2026
Revised: March 27, 2026
Accepted: April 3, 2026

In such difficult-to-treat cancers where even trimodal therapy (chemotherapy + immunotherapy + radiotherapy) could not improve survival, generating a tumor-targeted immune reaction could be a strategy to induce a systemic abscopal response that can also impact distant unirradiated tumor sites.[12] Using heavy metals like gold (Au) can be beneficial in augmenting the intracellular ROS production in radiotherapy due to the multiple interactions of their larger atoms with the radiation.[13] Gold nanoparticles (AuNPs), besides being biocompatible and easy to synthesize, can increase ROS production while suppressing the activation of ROS-regulating mechanisms even without radiation.[14,15] Meanwhile, accumulated ROS is also an internal factor involved in polarizing macrophages to the M1 phenotype, and such polarization has been observed when macrophages are exposed to proton radiation.[16−18] However, several studies have shown that macrophage polarization effects depend on the radiation type and dose due to the difference in the metabolic consequences, with high doses promoting immunosuppressive M2 TAMs and low doses stimulating M1 polarization.[16,19−22] These effects are also dependent on the polarization status of macrophages being exposed to radiation because of the intrinsic differences in their radiosensitivity.[23]

We hypothesized that the AuNP-mediated boosting of intracellular ROS production induced by medium-dose irradiation could be advantageous in repolarizing TAMs to the M1 pro-inflammatory type, potentially encouraging an anti-cancer immunogenic response. Our aim was to instigate this effect in macrophages using AuNPs alone or in combination with X-ray or proton irradiation and to assess if the consequent M1 repolarization played a role in the interaction of the macrophages with pancreatic cancer cells. To identify the most efficient AuNPs to fulfil this purpose, we tested AuNPs of two sizes—50 nm for high uptake and 15 nm for high radiosensitization. For coating the nanoparticles, we also tested two polymers—polyvinylpyrrolidone (PVP) and polyethylene glycol (PEG), FDA-approved polymers commonly used as delivery vehicles and stabilizers in pharmaceutical and cosmetic formulations.[24,25] We demonstrated the ability of 15 and 50 nm AuNPs to repolarize M2 macrophages to the M1 type, independently and in combination with 5 or 10 Gy X-ray irradiation, but not with proton irradiation. M2 macrophages loaded with 50 nm AuNPs coated with PVP could successfully reduce pancreatic cancer cell viability in co-cultures. The surface coating and size of the AuNPs and the dose and type of irradiation are important parameters for the outcome of this combined treatment.

2. EXPERIMENTAL SECTION

2.1. Preparation of Polymeric Coatings

Polyvinylpyrrolidone 29 kDa (PVP, Sigma-Aldrich) was carboxylated by heating PVP (2 g) dissolved in NaOH solution (100 mL, 0.1 N, Sigma-Aldrich) for 48 h at 140 °C in a hydrothermal autoclave (Cambridge Energy Solutions).[26] The opened pyrrolidone ring was stabilized by adding 35% formaldehyde (6 mL, VWR Chemicals), the pH was adjusted to 9, and the solution was cooled to 0 °C. Sodium borohydride (1.5 mg, Sigma-Aldrich) was added to the solution and stirred for 45 min at room temperature. The functionalized PVP was then lyophilized (Labconco FreeZone) and reconstituted to a 10 mM solution in ultrapure water for coating.

Lipoic acid-PEG-COOH 1 kDa (PEG, Biopharma PEG) was reconstituted to a 10 mM solution in a 1:1 mixture of ethanol (Sigma-Aldrich) and ultrapure water.

2.2. Synthesis of AuNPs

15 nm AuNPs were synthesized using the reverse Turkevich method.[27] Briefly, a solution of sodium citrate tribasic hydrate in ultrapure water (24.75 mL, 5.28 mM, pH 7.5, Sigma-Aldrich) was brought to a boil, and $HAuCl_4.3H_2O$ in ultrapure water (250 μL, 25.4 mM, pH 1.6, Sigma-Aldrich) was added to it. The solution was subjected to heated stirring till it turned red. Once cooled, ligand exchange coating was done by adding PVP (500 μL) or PEG (500 μL) and stirring overnight to form 15 nm AuNPs coated with PVP (15-PVP) or 15 nm AuNPs coated with PEG (15-PEG), respectively.

For synthesizing 50 nm particles, a seeded growth method was employed based on the classic Turkevich method.[28] First, gold nanoparticle seeds were prepared by bringing ultrapure water (48 mL) to boil, followed by the addition of $HAuCl_4.3H_2O$ (500 μL, 25 mM) and 1% sodium citrate tribasic hydrate (1.5 mL), and heated stirring for 30 min. Then, 50 nm AuNPs were prepared by boiling ultrapure water (45.5 mL) to which Tris (2 mL, 0.1 M, Sigma-Aldrich), 2 mL of the previously prepared seed solution, and $HAuCl_4.3H_2O$ (500 μL, 25 mM) were added and subjected to hot stirring for 30 min. After it cooled, PVP (107 μL) or PEG (427.5 μL) was added to the AuNP solution and stirred overnight to form 50 nm AuNPs coated with PVP (50-PVP) or 50 nm AuNPs coated with PEG (50-PEG), respectively, via ligand exchange coating.

The AuNP colloidal solutions were then purified and concentrated using 10 or 50 kDa centrifugal filters (Sartorius). Concentrated AuNP solutions in ultrapure water were stored at 4 °C and bath sonicated (Elma) at 35 kHz for 15 min before adding to cells.

2.3. Characterization of AuNPs

All characterizations were performed by diluting the AuNP suspensions in ultrapure water. UV–Vis spectroscopy was performed by measuring the absorbance of the AuNPs using a UV–Vis spectrophotometer (Thermo Scientific Genesys 50). For transmission electron microscopy (TEM), AuNP suspensions (3 μL) were deposited on TEM grids (Formvar copper/carbon 200 mesh, Ted Pella Inc.) and observed using a transmission electron microscope (FEI TECNAI 10) at a 100 kV acceleration voltage. The core diameters of the AuNPs were measured using the Particle Sizer plugin in Fiji software; at least 100 nanoparticles were measured in each group.

For visualizing the polymer coating, negative staining was performed by adding uranyl acetate (5 μL, SPI Chem) on the grids with AuNPs for 5 min, followed by blotting of excess, rinsing in a droplet of water (30 μL), and allowing the grid to air dry. These stained AuNPs were observed by high-resolution TEM (FEI TECNAI G^2 20) at a 120 kV acceleration voltage. Surface charge, hydrodynamic diameter, and polydispersity indices were assessed by ζ-potential and dynamic light scattering measurements (Malvern Zetasizer). For analyzing the AuNP constitutions by thermogravimetric analysis, 50 μL of AuNP solutions was loaded on sapphire crucibles (Mettler Toledo), and mass distributions were obtained by heating the samples from 100 to 800 °C at a rate of 10 °C min^{-1} in a TGA/DSC 3+ analyzer (Mettler Toledo) with the injection of 60 mL min^{-1} dry air and 20 mL min^{-1} nitrogen. The mass quantifications were performed using the STARe evaluation software (Mettler Toledo). To obtain the concentrations of the purified AuNP solutions, they were solubilized in aqua regia (1:3 mixture of HNO_3 (Carl Roth) and HCl (Carl Roth)) diluted to 1:3 with ultrapure water, followed by Au absorbance measurements by atomic absorption spectroscopy (Shimadzu). The concentrations were obtained by plotting the absorbance against a calibration curve made using a Au standard (1 g L^{-1}, Carl Roth).

2.4. Cell Culture and Maintenance

Immortalized bone-marrow-derived M0 macrophage cell line originating from *Mus musculus* C57BL/6 J was obtained from the laboratory of Dr. Howard A. Young, National Cancer Institute/NIH (Kerafast, ENH166-FP). Heat-inactivated serum (HIS) was prepared by heating

https://doi.org/10.1021/acsabm.6c00342
ACS Appl. Bio Mater. XXXX, XXX, XXX−XXX

fetal bovine serum (Sigma-Aldrich) at 58 °C for 30 min. L-929-conditioned medium was prepared by culturing the L-929 fibroblast cell line (ATCC, CCL-1) for 7 days in high-glucose Dulbecco's Modified Eagle Medium (DMEM, Gibco), supplemented with 10% HIS and 10% penicillin–streptomycin (Gibco), followed by filtering the media through 0.2 μm membrane filters (Sarstedt). High-glucose DMEM supplemented with 10% HIS, 10% L-929 conditioned medium, and 1% penicillin–streptomycin served as macrophage medium. Macrophages were polarized to an M2-like phenotype (M2) by exposing them to 20 ng mL^{-1} each of interleukin-13 (R&D Systems) and interleukin-4 (R&D Systems) in macrophage medium (M2-polarizing medium) for 24 hours. All cells were maintained at 37 °C with 5% CO_2. KPC pancreatic cancer cell line originating from C57BL/6 J mice (CancerTools.org, 153474) was maintained in high-glucose DMEM supplemented with 10% HIS and 1% penicillin–streptomycin (KPC medium). Cells were maintained at 37 °C with 5% CO_2.

2.5. Viability Assay

M0 macrophages were counted (NanoEntek) and seeded in a 96-well plate (4000 cells per well, Corning) in M2-polarizing medium, incubated for 24 h, and then exposed to 0, 6.25, 12.5, 25, 50, or 100 μg mL^{-1} concentrations of AuNPs for another 24 h. Then, the wells were rinsed with fresh macrophage medium, and the MTS reagent (CellTiter 96 AQueous One Solution Cell Proliferation Assay, Promega) diluted 1:5 in medium was added to the wells, incubated for 1.5 h at 37 °C, and the absorbance was read at 490 nm using a spectrophotometer (Bio-Rad xMark). The absorbance readings were normalized to those of untreated macrophages to obtain viability %.

2.6. Internalization Assay

M2 macrophages were incubated with 50 μg mL^{-1} AuNPs in medium for 24 h in T75 flasks (5×10^6 cells per flask, Corning). This was followed by rinsing with phosphate-buffered saline (PBS, Gibco), detaching the cells using 0.25% trypsin-EDTA (Gibco) and centrifuging them to obtain a cell pellet. This pellet was resuspended in 1 mL PBS, the cells were counted, and 1 mL of pure aqua regia was added. The cells were digested in the acid mix for 7 days at room temperature, after which atomic absorption spectroscopy was performed to determine the Au content as described earlier. With the known sizes, the obtained total Au mass in samples, and the cell counts, the internalization parameters were calculated for each sample as follows:

$$\text{Au concentration} = \frac{\text{Total Au mass}}{\text{Total number of cells}}$$

$$\text{Volume of AuNP} = \frac{4}{3}\pi r^3$$

$$\text{Mass of AuNP} = \text{Volume of AuNP} \times 1.93 \times 10^{-14}$$

$$\text{Total number of AuNPs} = \frac{\text{Total Au mass}}{\text{Mass of AuNP}}$$

$$\text{Number of AuNPs/cell} = \frac{\text{Total number of AuNPs}}{\text{Total number of cells}}$$

$$\text{Surface area of AuNP} = 4\pi r^2$$

$$\text{Exposed surface area} = \text{Number of AuNPs/cell} \times \text{surface area of AuNP}$$

where 1.93×10^{-14} μg nm^{-3} (19.3 g cm^{-3}) is the density of metallic Au and r is the radius of 1 AuNP.

2.7. Transmission Electron Microscopy of Macrophages

M2 macrophages were exposed to 50 μg mL^{-1} AuNPs for 24 h in T75 flasks (5×10^6 cells per flask). They were then pelleted and fixed in 3.2% glutaraldehyde (Thermo Scientific) for 2.5 h at 4 °C. The cells were washed 4 times in 1 mL sodium cacodylate buffer (Sigma Aldrich). Then, M2 macrophages were resuspended in 600 μL of a 1:1 mixture of osmium tetroxide (Thermo Scientific) and sodium cacodylate buffer and incubated for 1 h in a fume hood with light exposure. The cells were washed with cacodylate buffer, and dehydration was performed by exposing the cells to gradually increasing concentrations of ethanol (30%, 50%, 70%, 85%, 100%) for 30 min each. For embedding, first, the M2 macrophages were washed twice in 100% propylene oxide (Sigma-Aldrich), and the cell suspension was transferred to embedding capsules (BEEM, Agar Scientific). Then, the capsules were centrifuged, and the cell pellets were suspended in increasing concentrations (25%, 50%, 75%) of LX112 resin (Ladd Research Industries) dissolved in propylene oxide for 20 min each. Finally, pure LX112 was added and polymerized at increasing temperatures (37 °C and 45 °C for 48 h each) and then at 60 °C for 72 h. Sectioning was performed (Ultratome 8800 III, LKB Bromma), and the cell sections were mounted on copper/rhodium TEM grids (EM-Tec) and observed via TEM (FEI TECNAI 10) at a 60 kV acceleration voltage.

2.8. X-ray Irradiation

M2 macrophages (1×10^6 cells per well) polarized in 6-well plates (Corning) were exposed to 50 μg mL^{-1} AuNPs for 24 h, after which the medium was replaced with 2 mL of regular macrophage medium, and plates were irradiated with 5 or 10 Gy X-rays using an X-Rad 225 XL (PXi Precision X-ray) at 225 kVp and 13.5 mA to obtain a dose rate of 2 Gy min^{-1}. To irradiate KPC cells, the cells were seeded in 6-well plates (1×10^6 cells per well), and after 48 h, they were irradiated using the abovementioned method. Unirradiated cells with or without AuNPs served as controls.

2.9. Proton Irradiation

For proton irradiation, homemade irradiation chambers were used for cell culture (Figure S2a). The chambers had a hollow center to which polyethylene terephthalate Mylar of 3 μm thickness (GoodFellow) was adhered (EP21LV, MasterBond) to create a substrate for cell adhesion and growth. The chambers were sterilized by autoclaving. The Mylar surface on the interior face of the chamber was then coated with 0.5 μg mL^{-1} fibronectin (Bio-techne), 1 mL of M2-polarizing medium was added, and 5×10^5 M0 macrophages were slowly seeded along the center of the substrate. After allowing the cells to adhere for 3 h, the medium was removed, the chambers were quickly assembled to form a closed system, and 1 mL of M2-polarizing medium was filled in the chambers using a syringe (Terumo) and a 22G needle (Henke Sass Wolf). After 24 h of polarization, the medium was replaced with 1 mL macrophage medium with or without AuNPs and incubated for another 24 h. Then, the medium was again replaced with 3.5 mL of CO_2-independent medium (Gibco) supplemented with 10% HIS and 1% penicillin–streptomycin prior to irradiation. For irradiating KPC cells, 2×10^6 cells were seeded on Mylar coated with 0.1 μg mL^{-1} fibronectin and grown in KPC medium as explained above. After 48 h, before irradiation, the medium was replaced with CO_2-independent medium supplemented with 10% HIS and 1% penicillin–streptomycin.

The cells were irradiated with a proton beam generated by a 2 MV tandem accelerator (High Voltage Engineering Europa) at 5 or 10 Gy doses at a dose rate of 2 Gy min^{-1}.[29] The energy of the beam was set at 4 MeV to obtain a linear energy transfer of 10 keV μm^{-1} in water. The beam path of the proton irradiation setup is explained through the simulation shown in Figure S2b.[30] The simulation was performed using SRIM software (www.SRIM.org) with the following parameters: Ion: hydrogen; energy: 4000 keV; angle of incidence: 0; layers: silicon nitride—1 μm; air, dry—5000 μm; Mylar—3 μm; Water_Liquid—10,000 μm; total number of ions: 5000.

https://doi.org/10.1021/acsabm.6c00342
ACS Appl. Bio Mater. XXXX, XXX, XXX–XXX

2.10. Quantification of Gene Expression by RT-qPCR

Immediately after the proton irradiation, the M2 macrophages were trypsinized and transferred to 6-well plates. 24 h after X-ray or proton irradiation, macrophages were lysed, and RNA was extracted using the ReliaPrep RNA Tissue Miniprep System (Promega). The RNA was then reverse transcribed using the GoScript Reverse Transcription Mix Random Primers (Promega). qPCR was performed with a SYBR Green-based detection system GoTaq qPCR Master Mix (Promega) using the Viia 7 Real-time PCR system (Applied Biosciences). The primers (Integrated DNA Technologies) used are listed in Table S1. 40 s ribosomal protein S9 (RPS9) was used as the reference gene owing to its uniform expression among the experimental groups, and relative gene expressions were calculated by the $2^{-\Delta\Delta CT}$ method.

2.11. Survival Assay

For the co-culture experiments, KPC cells and M2 macrophages exposed to AuNPs were irradiated with 5 or 10 Gy X-rays or protons as mentioned earlier. After irradiation, the cells were detached, counted, and seeded in a 1:1 ratio of equally irradiated combinations (2×10^5 cells each) in a 24-well plate (Corning), e.g., M2+15 PVP irradiated with 5 Gy X-rays mixed with an equal number of KPC irradiated with 5 Gy X-rays. Imaging was performed every 2 h using the Incucyte live imaging system (Sartorius) for 48 h. Cell counts were obtained using the AI Cell Health module, and the counts at 48 h were normalized to those at 6 h to obtain the growth rates. To calculate the relative counts of KPC and KPC+M2, the growth rates of irradiated groups relative to those of untreated groups were calculated.

For macrophage monoculture experiments, the experimental setup was the same as above but only M2 macrophages were treated with AuNPs or not and then irradiated with 0,5 or 10 Gy X-rays or protons. Cell counts after reseeding were obtained using the Incucyte AI Cell Health module, and the counts at 48 h were normalized to those at 6 h to obtain the relative counts.

The co-culture seeding was also done once on another 24-well plate. 48 h post-irradiation, the cells were fixed with 4% paraformaldehyde (Sigma-Aldrich) for 10 min, followed by permeabilization with ice-cold methanol for 5 min. The cells were then incubated overnight in blocking buffer (0.5% bovine serum albumin in PBS), followed by another overnight incubation with anti-F4/80-APC (1:200, REAfinity, Miltenyi Biotec) diluted in blocking buffer. Nuclei were then stained by incubating the cells in 4,6-diamidino-2-phenylindole (1:10,000, Roche) diluted in blocking buffer for 1 h. The cells were washed twice with PBS, and 1 mL of ultrapure water was added per well. The cells were imaged on a Zeiss Cell Discoverer 7 confocal microscope equipped with an Airyscan detector and a 5×/0.25 NA Plan Apo dry objective. Images were then automatically quantified using Arivis Vision4D V4.1.1 software (Zeiss). Briefly, cells were segmented individually using a cellpose-based model and then sorted into two populations based on the mean fluorescence intensity of F4/80 labeling.

2.12. Statistical Analysis

All statistical analyses were performed using GraphPad Prism version 10.4.2. All data were analyzed by one-way or two-way ANOVA, followed by Bonferroni's multiple comparisons if the data had a normal distribution, and $y = \log(y)$ transformation was done if necessary. They were analyzed with the Kruskal–Wallis test, followed by Dunn's multiple comparisons, if the data did not have a normal distribution.

3. RESULTS AND DISCUSSION

3.1. Synthesis and Characterization of AuNP Cores

The citrate reduction method, also known as the Turkevich method, is a well-established technique to chemically synthesize AuNPs.[31] Research from Chithrani et al. demonstrated that the internalization of AuNPs was heavily dependent on the size and shape of the particles, with the 50-nm-sized spherical AuNPs having high internalization and retention in mammalian cells.[32,33] In the present study, 50 nm AuNPs were made by seeded growth, where AuNP seeds are first synthesized using the Turkevich method, which involves adding sodium citrate to a gold chloride solution. A second step of adding more reducing agent and gold chloride causes nucleated growth of the seeds, increasing the AuNP core size.[28]

Additionally, it has been established that 10 nm AuNPs are efficient in radiosensitizing cancer cells.[14,15,34] To keep the size as similar as possible, the inverse Turkevich method (reversing the order of adding ingredients, i.e., adding gold chloride to a sodium citrate solution) was used to create the 15 nm AuNP.[27] The AuNPs were then coated with either PEG or PVP via ligand exchange, yielding the various AuNPs used in the study, as described in Figure 1a, namely, 15 nm AuNP-PVP (15-PVP), 15 nm AuNP-PEG (15-PEG), 50 nm AuNP-PVP (50-PVP), and 50 nm AuNP-PEG (50-PEG). This easy method of coating was successful because of the high affinity that PEG and PVP have for Au. PVP gets adsorbed on the Au surface to form the coating, while the thiol group of PEG covalently bonds with Au on the surface for AuNP capping.[35,36]

Using the UV–vis absorption spectra (Figure 1b), the surface plasmon resonance peak (SPR, observed as absorbance peaks) for 15 nm AuNPs was observed at a 522 nm wavelength, typical for gold, which remained unchanged after coating with PVP; however, a small red shift to 524 nm was observed after PEG coating. The SPR peak for 50 nm AuNP was observed at a 530 nm wavelength, which also remained unchanged for 50-PVP but slightly shifted to 532 nm for 50-PEG.

According to the TEM observations (Figure 1c), the AuNPs were spherical and uniform in structure with no aggregation. Their core sizes were measured. Diameters of 14 ± 1.4 nm, 15.8 ± 2.6 nm, 47.6 ± 4 nm, and 50.5 ± 6.5 nm were determined for 15-PVP, 15-PEG, 50-PVP, and 50-PEG, respectively. The PEG-coated AuNPs had a wider size distribution than their PVP-coated counterparts, as shown in Figure 1d. These results indicated that while the PVP coating did not affect the AuNP cores, coating with PEG slightly increased the size and broadened the size distributions of the AuNP cores, probably because of its reducing property.[38] The PEG-enabled slight increase in Au core sizes explained the SPR peak red shift according to the Mie theory and was also observed by Cruje et al.[39,40]

3.2. High Coating Content Provides a Core–Shell Structure and Stability to AuNPs

TEM was repeated with uranyl acetate staining to observe the coatings. Uranyl acetate, being a heavy metal salt, acts as a negative stain to provide background contrast in TEM, enabling the visualization of the transparent organic coatings on the nanoparticles.[41] The classic core–shell structure of all four AuNPs was prominent, as seen in Figure 2a. Thermogravimetric analysis (Figure 2b) to identify the mass distributions showed that 15-PVP and 50-PVP AuNPs consisted of 93.8 and 46.5% PVP, respectively. 15-PEG and 50-PEG AuNPs contained 45.1 and 10.4% PEG, respectively. There was a notable increase in the hydrodynamic diameters of the 15 nm and 50 nm AuNPs after the polymer coating (Figure 2c and Table 1). ζ-potential measurements of AuNPs in ultrapure water revealed a shifted but still high negative surface charge on all AuNPs (Table 1). Even though 15-PVP had a surface charge lower than the other

https://doi.org/10.1021/acsabm.6c00342
ACS Appl. Bio Mater. XXXX, XXX, XXX–XXX

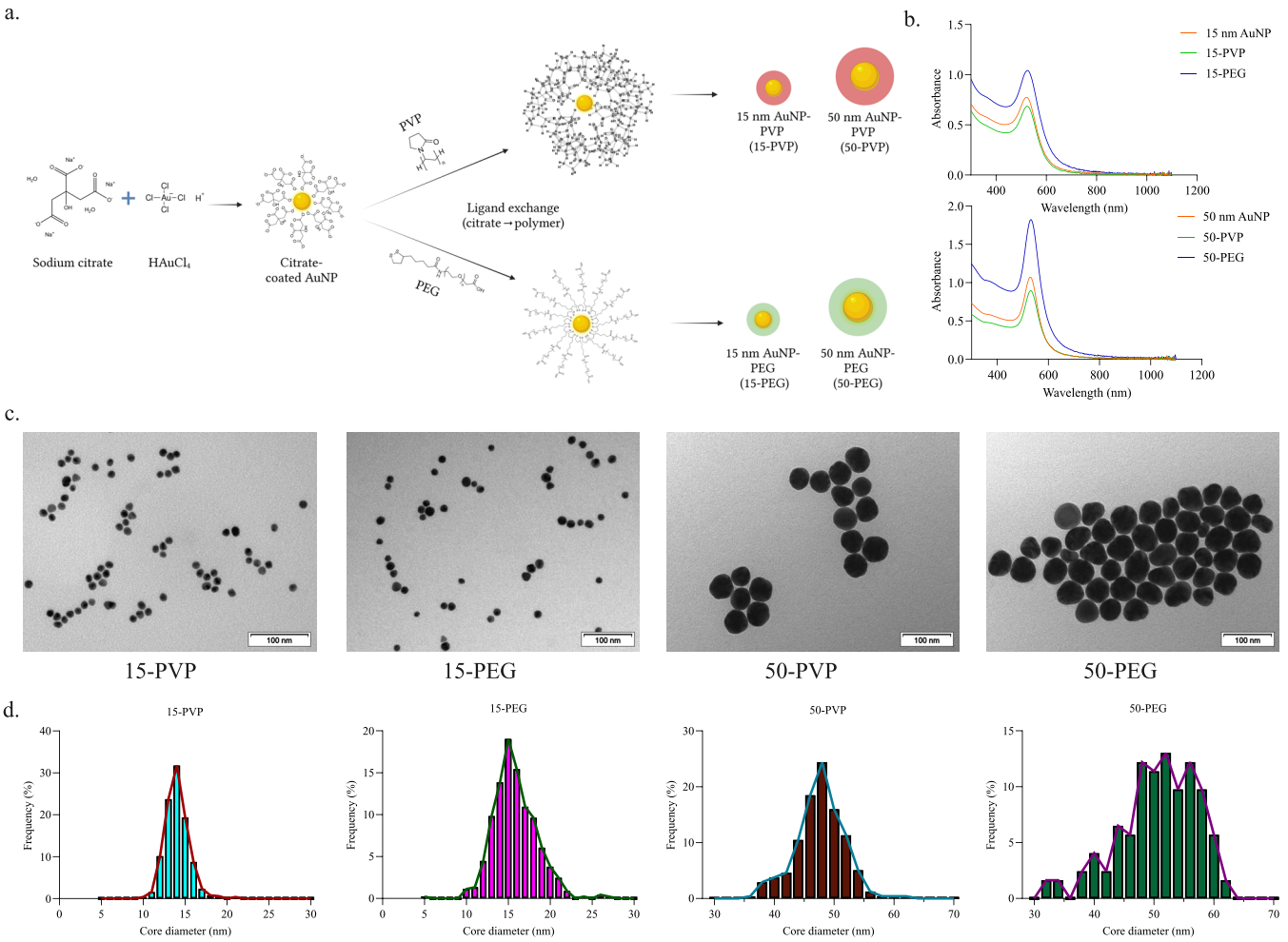

Figure 1. Synthesis of AuNPs and core characterization. (a) Citrate reduction method was used to synthesize AuNPs of 15 and 50 nm. After the initial synthesis, the citrate coating was replaced with PEG or PVP via ligand exchange to yield different AuNPs. The schematic representation was created in BioRender. Delcourt, B. (2025) https://BioRender.com/b62z847; the structure of PVP coating on AuNPs was adapted from ChemTube3D, and other chemical structures were obtained from their respective manufacturers.[37] (b) UV–Vis absorbance peaks before and after ligand exchange coating for the 15 nm AuNPs (top) and the 50 nm AuNPs (bottom). (c) TEM images of the AuNPs and (d) their size distributions.

AuNPs, no aggregation was observed in the duration of this study. The polydispersity indices of all AuNPs were low, as measured with dynamic light scattering, confirming their monodisperse and narrow size distributions (Table 1).

Overall, the AuNPs were deemed to be well-coated with PVP or PEG, and the coatings imparted high stability in their aqueous colloidal suspension forms. The AuNPs had typical core–shell structures where the PVP shells constituted a larger proportion of the nanoparticles than the PEG, which may be because of the difference in the molecular weight of the polymers (29 kDa PVP vs 1 kDa PEG) used in the coatings. The shifts in the hydrodynamic diameters and the ζ-potential confirmed the exchange of the citrate coating. Electrostatic repulsion and steric hindrance between the surface polymers play an essential role in imparting stability to these nanoparticles.[24,42]

3.3. AuNPs Are Non-Toxic to Macrophages, and PVP Coating Increases AuNP Internalization

To assess the possible toxicity of AuNPs, M2 macrophages were exposed to different AuNPs at concentrations ranging from 0 to 100 μg mL^{-1} for 24 h. Then, an MTS assay was performed to analyze the viability of the macrophages (Figure 3a). No reduction in viability was observed with the AuNPs at any concentration within the range tested, confirming their biocompatibility. As 100 μg mL^{-1} 50-PVP seemed to increase the viability of macrophages, which could also have been an effect of the interference with the assay readout due to high nanoparticle uptake, and because the effects of these AuNPs within M2 in combination with radio/proton therapy were unknown, we decided to use 50 μg mL^{-1} AuNP as a suitable non-toxic concentration for further experimentation.

Next, to investigate the cellular uptake of the AuNPs, M2 macrophages were incubated with 50 μg mL^{-1} AuNPs for 24 h, followed by acidic digestion and analysis of the Au mass in the samples using atomic absorption spectroscopy. Since the exposed AuNP surface was expected to determine their effect on the macrophages, we calculated the AuNP quantity and Au content inside the M2 macrophages (Figure 3b). As expected, the coating was the deterministic factor in the AuNP uptake. The exposed surface area, Au concentration, and number of 15-PVP AuNPs were 32-fold higher than those

https://doi.org/10.1021/acsabm.6c00342
ACS Appl. Bio Mater. XXXX, XXX, XXX–XXX

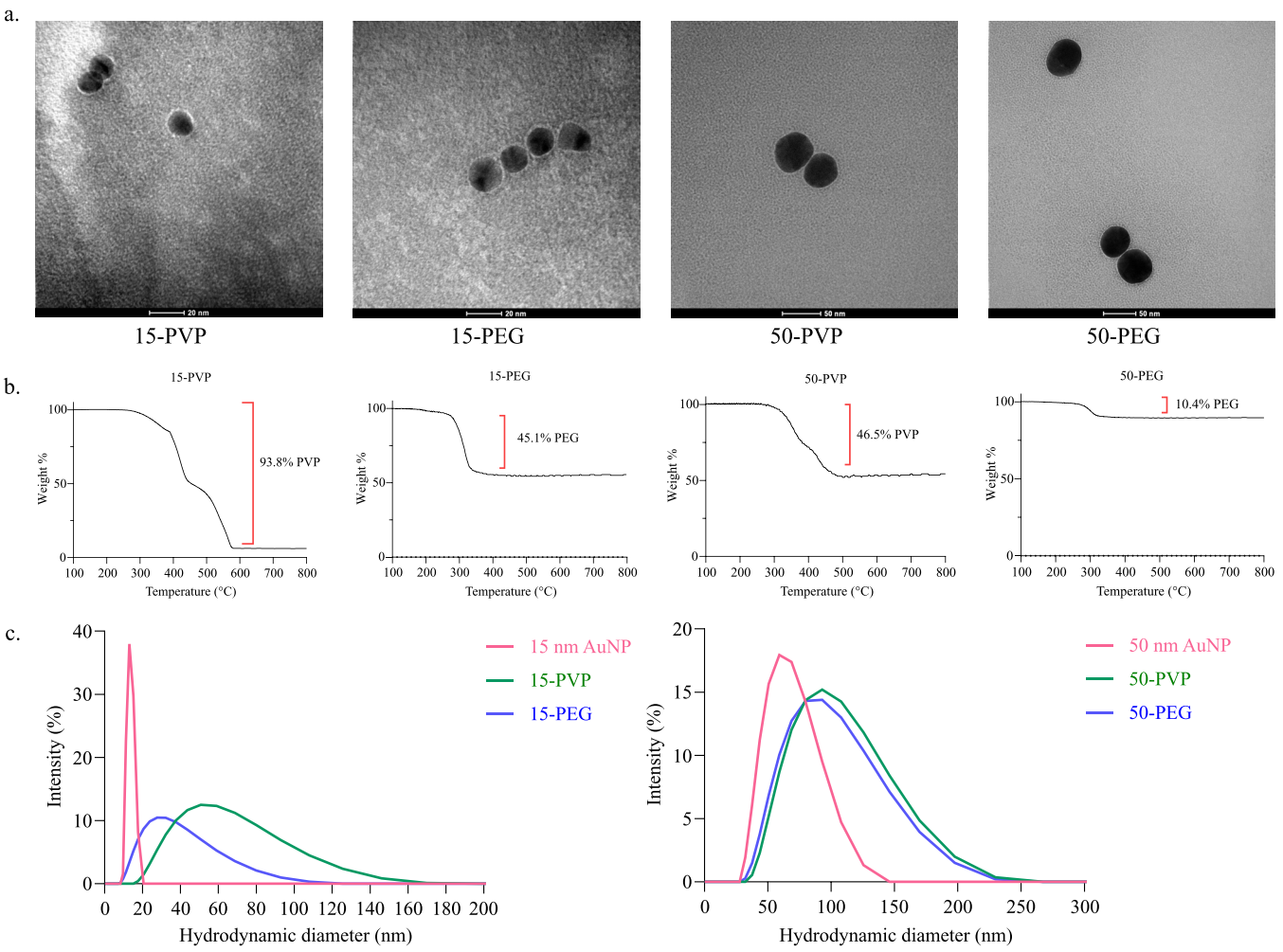

Figure 2. Characterization of the polymer shells of AuNPs. (a) Negative staining of AuNPs with uranyl acetate, followed by TEM. (b) Thermogravimetric analyses of AuNPs. (c) Hydrodynamic diameters of AuNPs suspended in ultrapure water evaluated using dynamic light scattering.

Table 1. Measurement of Hydrodynamic Diameters, ζ-Potential (Indicating Surface Charge), and Polydispersity Indices of the AuNPs before and after Polymer Coating

AuNP	hydrodynamic diameter [nm]	ζ-potential [mV]	polydispersity index
15 nm AuNP	13.6	−22.8	0.54
15-PVP	58.46	−15.38	0.26
15-PEG	34.26	−22.75	0.32
50 nm AuNP	65.25	−35.87	0.12
50-PVP	98.37	−25.49	0.14
50-PEG	92.88	−24.52	0.19

of 15-PEG. The internalized 50-PVP AuNPs had a 25-fold higher exposed surface area, Au concentration, and quantity compared to 50-PEG. For both coatings, there was a significantly higher number of internalized AuNPs for the 15 nm particles than for their 50-nm-sized counterparts.

This was corroborated by TEM observations (Figure 3c), where M2 incubated with 15-PVP and 50-PVP not only displayed abundant visible accumulation of AuNPs within the cells but also appeared clustered in intracellular vesicles, indicative of classic endocytosis. On the other hand, fewer PEG-coated particles were internalized by M2 macrophages and were mostly found dispersed within the cells. The low internalization of the PEG-coated AuNPs can be attributed to the "stealth effect" that PEG imparts to nanoparticles because of its conformation and surface density, enabling them to escape being recognized by macrophages by preventing the serum proteins from forming a protein corona around the AuNPs.[43,44] The high uptake of PVP-AuNPs by macrophages in this work correlates with studies that have shown that PVP-coated AuNPs adsorb more serum proteins than PEG-coated nanoparticles, encourage higher uptake by macrophages, and improve clearance from injected tissues.[45−47]

https://doi.org/10.1021/acsabm.6c00342
ACS Appl. Bio Mater. XXXX, XXX, XXX−XXX

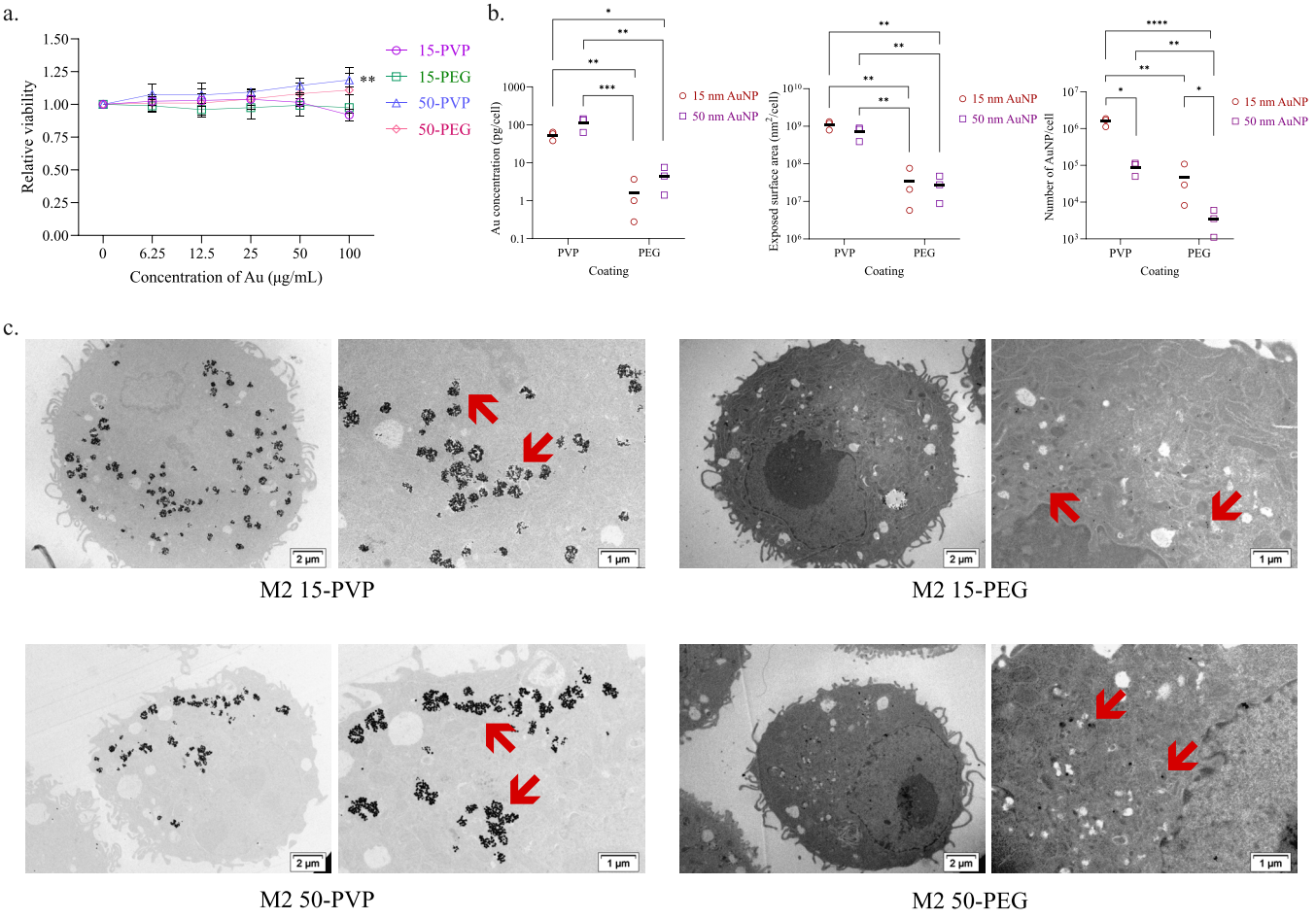

Figure 3. Assessment of toxicity and internalization of AuNPs in macrophages. (a) M2 macrophages were incubated with AuNPs for 24 h, and the viability was assessed by MTS assay. Results are presented as means ± 1 standard deviation ($n = 3$). (b) Internalization studies were conducted by exposing M2 macrophages to 50 μg/mL AuNPs for 24 h, followed by aqua regia digestion and atomic absorption spectroscopy to quantify the internalized Au mass. Au mass and cell counts were used to calculate the internalized Au concentration, exposed surface area, and the number of AuNPs/cell. Mean values are indicated by horizontal lines within each group ($n = 3$). (c) AuNPs inside M2 macrophages were visualized using TEM and are indicated with red arrows. Statistical analyses were performed using one-way ANOVA, followed by Bonferroni's multiple comparison test or Kruskal–Wallis test with Dunn's multiple comparison test as appropriate; $*p \leq 0.05$, $**p \leq 0.01$, $***p \leq 0.001$, $****p < 0.0001$.

3.4. AuNPs Alone and in Combination with X-rays Can Repolarize M2 Macrophages toward an M1 Phenotype

Low-to-moderate proton irradiation doses between 2 and 10 Gy can establish a pro-inflammatory environment by upregulating M1 markers and immunogenic cell death markers.[16,48] Proton irradiation above 14 Gy total dose promotes an M2-like phenotype, evidenced by a decrease in the expression of M1 markers like Interleukin-6 and Interleukin-8, and an increase in anti-inflammatory markers like arginase-1, which is more pronounced for doses above 20 Gy. X-ray doses higher than 10 Gy also cause an influx of circulating macrophages into the tumor microenvironment, which then polarize into the pro-tumoral M2 phenotype, aiding in angiogenesis and faster tumor growth.[48] Therefore, in this work, we irradiated cells with 5 or 10 Gy doses to retain the immunogenic effect of radiation.

To understand the effect of X-rays and AuNPs on the polarization of M2 macrophages, we exposed M2 macrophages to AuNPs for 24 h and then irradiated with 0, 5, or 10 Gy X-rays. 24 h post-irradiation, the cells were lysed, and the mRNA levels of M1-associated genes chemokine (C-X-C motif) ligand 10 (CXCL10), macrophage receptor with collagenous structure (MARCO), tumor necrosis factor-α (TNF-α), cluster of differentiation 86 (CD86), and M2-associated marker cluster of differentiation 206 (CD206) were assessed. Besides these typical macrophage markers, the expenditure of redox enzymes in managing the post-treatment ROS might lead to a depletion of the intracellular concentration of these enzymes, which would require replenishment by increased enzyme synthesis. Hence, we also evaluated the genes for redox-management enzymes thioredoxin reductase (TRXR1), glutathione peroxidase (GPX1) and superoxide dismutase (SOD1) to understand the ROS-management enzymes involved.

X-ray irradiation alone upregulated CXCL10 (Figure 4a) and MARCO (Figure 4b) expression in a dose-dependent manner. However, CD206 (Figure 4d) and GPX1 (Figure 4f) were also upregulated after 10 Gy irradiation, suggesting a shift toward a mixed macrophage phenotype and that the neutralization of X-ray radiation-induced ROS could be dependent on glutathione peroxidase. There was no effect of X-rays alone on the expression of TNF-α (Figure 4c), TRXR1 (Figure 4e), CD86 (Figure S1a), or SOD1 (Figure S1b).

https://doi.org/10.1021/acsabm.6c00342
ACS Appl. Bio Mater. XXXX, XXX, XXX–XXX

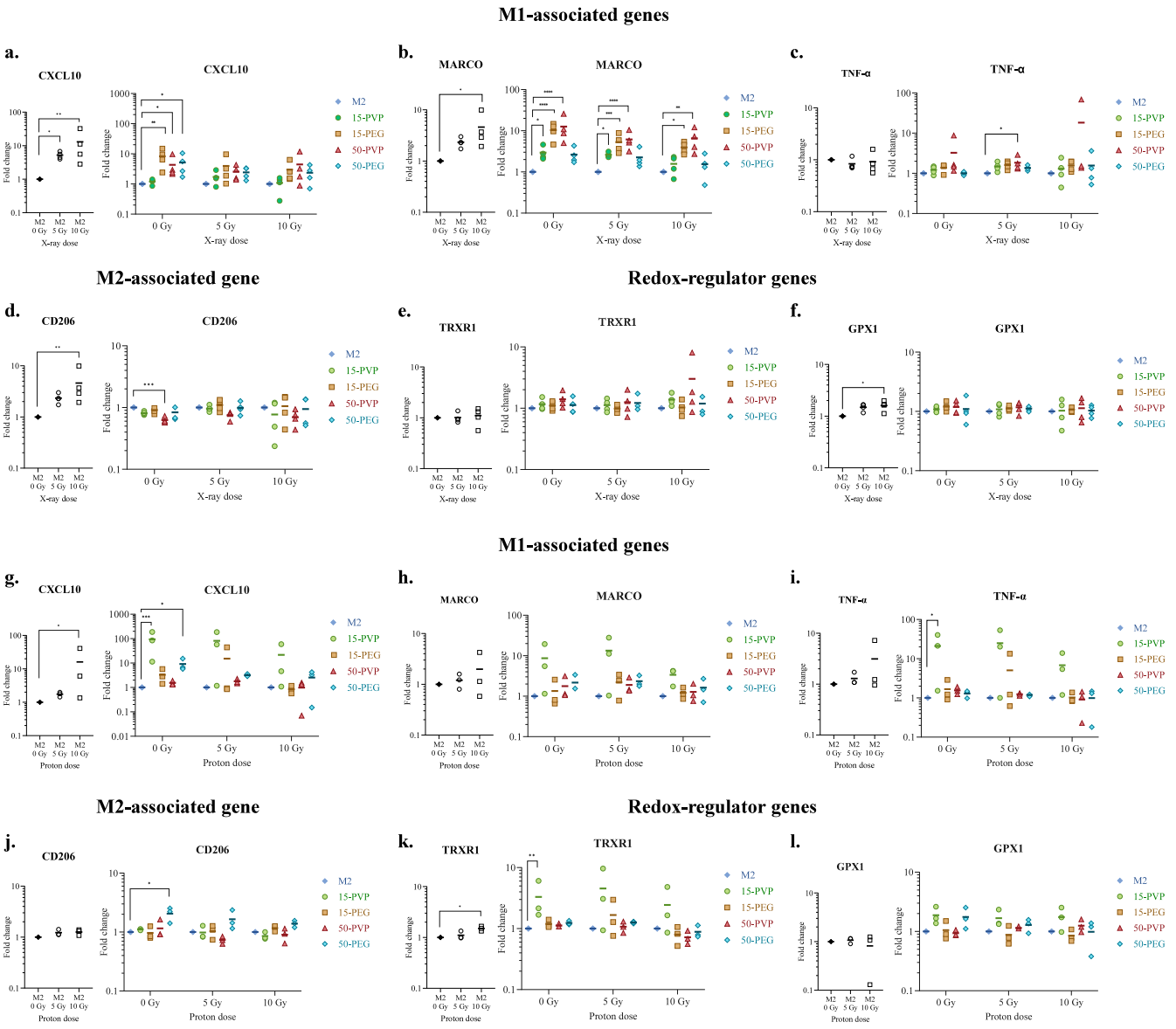

Figure 4. Effect of AuNPs on radiation-mediated polarization of macrophages. M2 macrophages were incubated with various AuNPs (or not) for 24 h and then exposed to 0, 5, or 10 Gy X-ray radiation. 24 h after irradiation, mRNA levels of M1 marker genes (a) CXCL10, (b) MARCO, and (c) TNF-α, (d) M2 marker gene CD206, and genes for the redox-regulating enzymes (e) TRXR1 and (f) GPX1 were assessed ($n = 4$). To test the effect of proton irradiation, M2 with or without AuNPs were exposed to 0, 5, or 10 Gy protons, and 24 h later, mRNA levels of (g) CXCL10, (h) MARCO, (i) TNF-α, (j) CD206, (k) TRXR1, and (l) GPX1 were evaluated ($n = 3$). In all datasets, the effects of radiation alone on M2 macrophages are presented in the left panels, with the irradiated groups normalized to untreated M2 macrophages. The right panels have M2+AuNPs normalized to M2 macrophages without AuNPs for each radiation dose group. Mean values are indicated by horizontal lines within each group. Statistical analyses were performed using one-way ANOVA, followed by Bonferroni's multiple comparisons or Kruskal–Wallis test with Dunn's multiple comparisons as appropriate; *$p \leq 0.05$, **$p \leq 0.01$, ***$p \leq 0.001$, ****$p < 0.0001$.

The AuNPs used in the study were independently capable of repolarizing M2 macrophages, and the effects varied with the size and coating. CXCL10 was upregulated in M2 macrophages by 15-PEG, 50-PVP, and 50-PEG independently of X-rays but did not have an additional effect when combined with X-ray irradiation (Figure 4a). Notably, MARCO was not only significantly upregulated by 15-PVP, 15-PEG, and 50-PVP AuNPs alone; however, the increased expression was further enhanced when combined with X-rays at 5 and 10 Gy doses (except for 15-PVP) (Figure 4b). The most important repolarizing effect was seen in M2 macrophages exposed to 50-PVP, in which all the M1 genes of interest were upregulated (alone or with X-rays), and CD206 was downregulated. No AuNP-based effect was observed on TRXR1, GPX1, and SOD1.

For studying the effect of AuNPs in combination with protons, M2 macrophages were seeded on homemade irradiation chambers, exposed to AuNPs and irradiated with 0, 5, or 10 Gy protons. They were then transferred to cell culture plates and lysed 24 h post-irradiation for mRNA analyses. There was an upregulation of CXCL-10 (Figure 4g) and TRXR1 (Figure 4k) when M2 macrophages were exposed to 10 Gy protons, indicating the potential role of thioredoxin reductase in

https://doi.org/10.1021/acsabm.6c00342
ACS Appl. Bio Mater. XXXX, XXX, XXX–XXX

managing proton irradiation-induced redox stress. There were small, non-significant increases in the expressions of TNF-α (Figure 4i) and MARCO (Figure 4h) as well, pointing toward an M1 shift upon 10 Gy proton exposure.

Interestingly, when M2 macrophages were pre-incubated with 15-PVP, there were also upregulations of CXCL10, TNF-α, and TRXR1. Although these additional effects were not statistically significant but still present after proton irradiation, the AuNPs did not seem to hinder the proton-induced M1 shift (no reduced expressions in M1 genes). The addition of 50-PEG increased the expression of CXCL10 and CD206 (Figure 4j), potentially triggering a mixed phenotype. There was no effect of protons alone or with AuNPs on the expression of GPX1 (Figure 4l), CD86 (Figure S1c), or SOD1 (Figure S1d).

The differences in the effects of AuNPs on unirradiated macrophages between the X-ray and proton experiments could be because of the different seeding conditions (use of a Mylar substrate) in our proton irradiation setup, which may also have been the reason for the high variability in the data. To minimize differences in irradiation protocols, the cell seeding density and the quantity of media containing polarizing cytokines or AuNPs were kept proportional to the surface area in both experiments, and the unirradiated groups were grown on the same substrate as the irradiated groups for optimal normalization. The variation in the expression of macrophage markers induced by the two types of irradiation and various AuNPs could be due to differences in the downstream pathways involved in the reprogramming, as there are many factors that govern macrophage polarization.[49] This was attested by the observed upregulation of two different redox-managing enzyme genes by the two types of radiation.

Antioxidants such as superoxide dismutase, carotenoids and thioredoxin reductase maintain intracellular homeostasis, which gets disrupted when there is generation of a very high quantity of ROS after irradiation.[50] Upon irradiation, elevated intracellular ROS levels in macrophages, along with the inflammatory factors of the tumor microenvironment, help to activate an M1-like phenotype. Signals that trigger and sense intracellular ROS production, such as inducible nitric oxide synthase and TNF-α, are also upstream actors for the induction of transcription factors involved in the synthesis and release of immunogenic cytokines, resulting in an inflammatory response.[51,52] Additionally, AuNPs have been observed to increase the intracellular ROS level in cancer cells by inhibiting cellular redox-management enzymes like thioredoxin reductase and glutathione peroxidase, even without irradiation.[14,53] In this study, we have demonstrated that the antioxidant systems activated after irradiation depend on the type and dose of radiation. Notably, 10 Gy X-ray exposure increased the glutathione peroxidase mRNA levels, 10 Gy proton exposure upregulated thioredoxin reductase, and neither seemed to affect the superoxide dismutase mRNA expression. However, we did not find any effect of AuNPs when used alone on the mRNA level of the antioxidant genes studied here.

3.5. 50-PVP-Containing M2 Macrophages Can Induce Cell Death in Pancreatic Cancer Cells Alone and with X-rays

Finally, we aimed to evaluate whether the induced reprogramming effect could influence the survival of murine pancreatic cancer cells obtained from LSL-Kras$^{G12D/+}$; LSL-Trp53$^{R172H/+}$; Pdx1-Cre (KPC) mice, an established model for pancreatic ductal adenocarcinoma.[54] For this experiment, 15-PVP and 50-PVP AuNPs were used because of their higher internalization and the M1-shift they generated alone and in combination with X-rays. KPC cells and M2 macrophages with or without AuNPs were irradiated alone in a 6-well plate, followed by detaching, counting, and adding the cells in appropriate combinations in a 24-well plate, followed by live microscopy. 10 Gy X-rays reduced KPC cell counts; however, the addition of equally irradiated M2 to KPC in a 1:1 ratio generated a further reduction in the total population, not just with 10 Gy but also with 5 Gy X-rays (Figure 5a).

More importantly, we observed a marked reduction in the total cell counts of co-cultures containing KPC cells and M2 macrophages with 50-PVP, compared to the untreated group without irradiation, and compared to 15-PVP with 5 Gy X-rays (Figure 5b). The 15-PVP exposure did not alter the behavior of the cells. Therefore, the presence of irradiated macrophages can make even the lowest dose of 5 Gy X-rays more cytotoxic and enhance the toxicity of 10 Gy X-rays. All co-culture groups with AuNPs displayed an X-ray dose-dependent reduction in cell population, while pre-exposure of the M2 macrophages to 50-PVP reduced it further, demonstrating the cytotoxic effect of macrophages repolarized by 50-PVP and X-ray radiation. Results of the statistical analyses are displayed in Table S2.

For assessing the effect of protons on the co-culture setup, we performed the same procedure but using proton irradiation chambers. Irradiation with 5 Gy protons did not induce any significant change in the number of KPC cells; however, the cytotoxic effect of 10 Gy protons on KPC cells was more pronounced when equally irradiated M2 macrophages were added to them (Figure 5a). When the M2 macrophages were pre-exposed to AuNPs, a significant reduction in cell count was observed with 10 Gy proton irradiation for all co-culture groups; however, the AuNPs did not have any additional effect on the killing effect of proton irradiation (Figure 5b).

To assess if the cytotoxicity observed in the co-cultures was because of the death of macrophages, we performed the same experiment as above in M2 macrophage monocultures. It was observed that irradiation with X-rays or protons was cytotoxic at 5 and 10 Gy doses for macrophages exposed or not to AuNPs (Figure 5c). Importantly, there were no additional effects caused by AuNPs on the macrophage population counts. This confirmed that the cytotoxicity observed in co-cultures containing M2 macrophages exposed to 50-PVP alone and in combination with 5 Gy X-rays (Figure 5b) was not due to toxic effects of AuNPs on the macrophages.

Using immunofluorescence labeling, we performed the same experiment as above and used anti-F4/80 to identify macrophages and distinguish the two cell types in the co-cultures. The labeling was performed 48 h post-irradiation (Figure S3). The F4/80$^-$ KPC cell counts were reduced in the presence of F4/80$^+$ macrophages, especially when the cells were irradiated with 5 or 10 Gy X-rays (Figure S3a,c) or 5 or 10 Gy protons (Figure S3b,d).

The correlation of the co-culture data with the M1 repolarization effects caused by 50-PVP alone and in combination with X-rays, as observed in Figure 4, suggests that M1 repolarization of macrophages can contribute to cancer cell phagocytosis.[55] From the co-culture experiment shown in Figure 5, it can be concluded that, while the addition of irradiated M2 macrophages to KPC had decreased the number of viable cells, the

https://doi.org/10.1021/acsabm.6c00342
ACS Appl. Bio Mater. XXXX, XXX, XXX−XXX

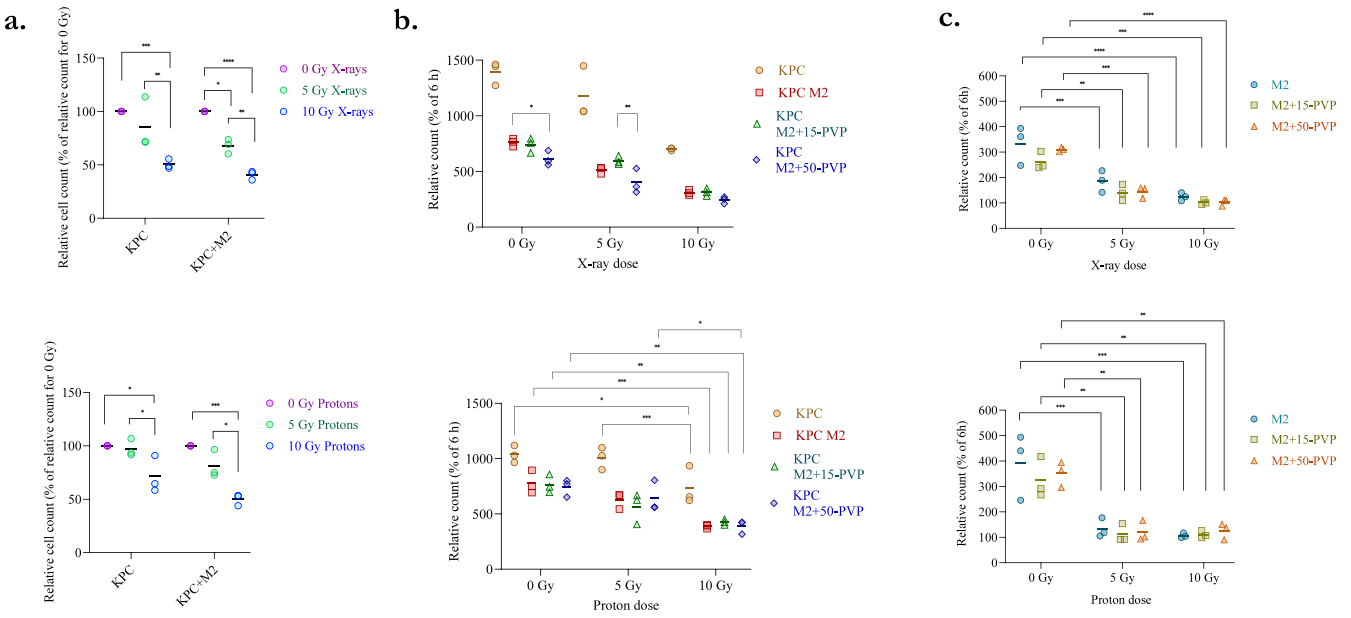

Figure 5. Effect of AuNPs and radiation in pancreatic cancer cells co-cultured with macrophages. M2 macrophages were exposed to AuNPs for 24 h, after which they were irradiated with 0, 5, or 10 Gy X-rays or protons ($n = 3$). Meanwhile, KPC pancreatic cancer cells were also irradiated with the same doses. After irradiation, both types of cells were detached and reseeded in equally irradiated combinations in a 1:1 ratio. For 48 h, the total cell counts were evaluated by live microscopy. (a) Relative cell counts of irradiated KPC-only and KPC+M2 groups at 48 h post-irradiation relative to those of unirradiated cells. (b) Relative counts using the cell counts at 48 h compared to those at 6 h post-reseeding. (c) M2 macrophages were exposed to AuNPs for 24 h, irradiated with 0, 5, or 10 Gy X-rays or protons and then reseeded. For 48 h, the total cell counts were assessed, and relative counts were calculated using the cell counts at 48 h compared to those at 6 h post-reseeding. Mean values are indicated by horizontal lines within each group. Statistical analyses were performed using one-way ANOVA, followed by Bonferroni's multiple comparisons; *$p \leq 0.05$, **$p \leq 0.01$, **$p \leq 0.001$, ****$p < 0.0001$.

internalization of 50-PVP nanoparticles by the M2 cells further decreased the number of viable cells when combined with X-rays, but not with protons.

4. CONCLUSIONS

Targeting the immune cells in cancer has been a hot topic for the past few decades and so has the application of nanomaterials in the delivery of chemotherapeutics and immunomodulators, both showing incredible successes in establishing improved patient outcomes. In this study, we used gold nanoparticles for macrophage repolarization using their ROS-inducing effects. Both synthesis methods used in this work are not only simple but can also be customized to create AuNPs of the desired size by altering the ratio of Au and citrate and are scalable to increase production by up to 8 times. The presence of –COOH groups on both polymer coatings makes it possible to conjugate targeting antibodies to functionalize these AuNPs and has also been shown to promote preferential uptake by macrophages.[26,56] In our study, while the cytotoxic effect appeared to be centered around the type and dose of irradiation, the presence of irradiated macrophages, especially those pre-incubated with 50-PVP AuNPs, boosted the M1 repolarization and the toxicity of X-rays on KPC cells. Both types of irradiation showed success in repolarizing TAMs. 50-PVP AuNPs combined with 5 Gy X-ray radiation appear to have the best M1 repolarization effect while also being cytotoxic for pancreatic cancer cells, hence proving its potential to be a promising two-pronged strategy for killing pancreatic cancer cells by enhancing the anti-tumoral effects of TAMs.

Further studies will focus on assessing the translatability of our approach using in vivo experiments to analyze the AuNP retention dynamics and the immunological and cytotoxic effects of the 50-PVP+X-rays combination on the treated tumor and its microenvironment, as well as untreated distal tumors, considering the various interactions that macrophages have in the cancer scenario.[6] In conclusion, 50-PVP nanoparticles can be a safe and effective way to improve radiotherapy for treating pancreatic cancer by establishing an immunogenic switch in TAM behavior even at moderate doses, additionally reducing the harmful side effects of high-dose radiotherapy. To our knowledge, this is the first reported use of AuNP + irradiation combination treatment for manipulating macrophages in cancer radiotherapy. The feasible synthesis of the AuNPs and the global prevalence of X-ray radiotherapy centers can aid in the potential translation of this strategy to improve the treatment of pancreatic cancer patients.

■ ASSOCIATED CONTENT

Data Availability Statement

The data that support the findings of this study are available from the corresponding author upon reasonable request.

Supporting Information

The Supporting Information is available free of charge at https://pubs.acs.org/doi/10.1021/acsabm.6c00342.

Additional experiments and experimental details, including photograph and simulation of the proton irradiation setup (DOCX)

https://doi.org/10.1021/acsabm.6c00342
ACS Appl. Bio Mater. XXXX, XXX, XXX–XXX

AUTHOR INFORMATION

Corresponding Author

Shalini Iyer – *Physics Department, Namur Research Institute for Life Sciences (NARILIS), University of Namur, Namur 5000, Belgium; Research Unit in Cell Biology (URBC), NARILIS, University of Namur, Namur 5000, Belgium;* orcid.org/0000-0003-3587-3605; Email: shalini.iyer@unamur.be

Authors

Tijani Tabarrant – *Physics Department, Synthesis, Irradiation and Analysis of Materials Platform (SIAM), University of Namur, Namur 5000, Belgium*

Benjamin Ledoux – *Morph-Im Platform, University of Namur, Namur 5000, Belgium*

Carine Michiels – *Research Unit in Cell Biology (URBC), NARILIS, University of Namur, Namur 5000, Belgium;* orcid.org/0000-0002-9169-1294

Anne-Catherine Heuskin – *Physics Department, Namur Research Institute for Life Sciences (NARILIS), University of Namur, Namur 5000, Belgium;* orcid.org/0000-0002-4960-5284

Complete contact information is available at: https://pubs.acs.org/doi/10.1021/acsabm.6c00342

Funding

SI was a recipient of the Fonds de la Recherche Scientifique-FNRS Télévie under Grant No. 42733. TT and BL received institutional funding from the University of Namur. CM and A-CH were supported by the Région Wallonne, Belgium under Grant No. 7289 (ProtherWal). A-CH was also a recipient of the Fondation Universitaire. This article is published with the support of the Belgian University Foundation through a publication grant awarded to A-CH.

Notes

The authors declare no competing financial interest.

ACKNOWLEDGMENTS

The authors thank Corry Charlier for his guidance with the TEM imaging and Caroline De Bona for sample sectioning. They are thankful to Dr. Nikolay Tumanov for his help with the thermogravimetric analyses. They also thank the technological platforms SIAM, electron microscopy, and Morph-Im at the University of Namur.

REFERENCES

(1) Zhu, H.; Chua, M. L. K.; Chitapanarux, I.; Kaidar-Person, O.; Mwaba, C.; Alghamdi, M.; Mignola, A. R.; Amrogowicz, N.; Yazici, G.; Bourhaleb, Z.; Mahmood, H.; Faruque, G. M.; Thiagarajan, M.; Acharki, A.; Ma, M.; Harutyunyan, M.; Sriplung, H.; Chen, Y.; Camacho, R.; Zhang, Z.; Abdel-Wahab, M. Global Radiotherapy Demands and Corresponding Radiotherapy-Professional Workforce Requirements in 2022 and Predicted to 2050: A Population-Based Study. *Lancet Global Health* **2024**, *12* (12), e1945–e1953.

(2) Bray, F.; Laversanne, M.; Sung, H.; Ferlay, J.; Siegel, R. L.; Soerjomataram, I.; Jemal, A. Global Cancer Statistics 2022: GLOBOCAN Estimates of Incidence and Mortality Worldwide for 36 Cancers in 185 Countries. *CA Cancer J. Clin.* **2024**, *74* (3), 229–263.

(3) Zhang, Z.; Liu, X.; Chen, D.; Yu, J. Radiotherapy Combined with Immunotherapy: The Dawn of Cancer Treatment. *Signal Transduction Targeted Ther.* **2022**, *7* (1), 1–34.

(4) Chen, Z.; Dominello, M. M.; Joiner, M. C.; Burmeister, J. W. Proton versus Photon Radiation Therapy: A Clinical Review. *Front. Oncol.* **2023**, *13*.

(5) Girdhani, S.; Sachs, R.; Hlatky, L. Biological Effects of Proton Radiation: What We Know and Don't Know. *Radiat. Res.* **2013**, *179* (3), 257–272.

(6) Belgiovine, C.; Digifico, E.; Anfray, C.; Ummarino, A.; Torres Andón, F. Targeting Tumor-Associated Macrophages in Anti-Cancer Therapies: Convincing the Traitors to Do the Right Thing. *J. Clin. Med.* **2020**, *9* (10), No. 3226.

(7) Mantovani, A.; Allavena, P.; Sica, A.; Balkwill, F. Cancer-Related Inflammation. *Nature* **2008**, *454* (7203), 436–444.

(8) Allemani, C.; Matsuda, T.; Carlo, V. D.; Harewood, R.; Matz, M.; Nikšić, M.; Bonaventure, A.; Valkov, M.; Johnson, C. J.; Estève, J.; Ogunbiyi, O. J.; Azevedo E Silva, G.; Chen, W.-Q.; Eser, S.; Engholm, G.; Stiller, C. A.; Monnereau, A.; Woods, R. R.; Visser, O.; Lim, G. H.; Aitken, J.; Weir, H. K.; Coleman, M. P.; Bouzbid, S.; Hamdi-Chérif, M.; Zaidi, Z.; Meguenni, K.; Regagba, D.; Bayo, S.; Bougadari, T. C.; Manraj, S. S.; Bendahhou, K.; Fabowale, A.; Bradshaw, D.; Somdyala, N. I. M.; Kumcher, I.; Moreno, F.; Calabrano, G. H.; Espinola, S. B.; Quintero, B. C.; Fita, R; Diumenjo, M. C.; Laspada, W. D.; Ibañez, S. G.; Lima, C. A.; Souza, P. C. F. D.; Pino, K. D.; Laporte, C.; Curado, M. P.; de Oliveira, J. C.; Veneziano, C. L. A.; Veneziano, D. B.; Latorre, M. R. D. O.; Tanaka, L. F.; Rebelo, M. S.; Santos, M. O.; Galaz, J. C.; Aravena, M. A.; Monsalve, J. S.; Herrmann, D. A.; Vargas, S.; Herrera, V. M.; Uribe, C. J.; Bravo, L. E.; Garcia, L. S.; Arias-Ortiz, N. E.; Morantes, D.; Jurado, D. M.; Chamorro, M. C. Y.; Delgado, S.; Ramirez, M.; Alvarez, Y. H. G.; Torres, P.; Martínez-Reyes, F.; Jaramillo, L.; Quinto, R.; Castillo, J.; Mendoza, M.; Cueva, P.; Yépez, J. G.; Bhakkan, B.; Deloumeaux, J.; Joachim, C.; Macni, J.; Carrillo, R.; Klincovstein, J. S.; Gomez, R. R.; Poquioma, E.; Tortolero-Luna, G.; Zavala, D.; Alonso, R.; Barrios, E.; Eckstrand, A.; Nikiforuk, C.; Noonan, G.; Turner, D.; Kumar, E.; Zhang, B.; McCrate, F. R.; Ryan, S.; MacIntyre, M.; Saint-Jacques, N.; Nishri, D. E.; McClure, C. A.; Vriends, K. A.; Kozie, S.; Stuart-Panko, H.; Freeman, T.; George, J. T.; Brockhouse, J. T.; O'Brien, D. K.; Holt, A.; Almon, L.; Kwong, S.; Morris, C.; Rycroft, R.; Mueller, L.; Phillips, C. E.; Brown, H.; Cromartie, B.; Schwartz, A. G.; Vigneau, F.; Levin, G. M.; Wohler, B.; Bayakly, R.; Ward, K. C.; Gomez, S. L.; McKinley, M.; Cress, R.; Green, M. D.; Miyagi, K.; Ruppert, L. P.; Lynch, C. F.; Huang, B.; Tucker, T. C.; Deapen, D.; Liu, L.; Hsieh, M. C.; Wu, X. C.; Schwenn, M.; Gershman, S. T.; Knowlton, R. C.; Alverson, G.; Copeland, G. E.; Bushhouse, S.; Rogers, D. B.; Jackson-Thompson, J.; Lemons, D.; Zimmerman, H. J.; Hood, M.; Roberts-Johnson, J.; Rees, J. R.; Riddle, B.; Pawlish, K. S.; Stroup, A.; Key, C.; Wiggins, C.; Kahn, A. R.; Schymura, M. J.; Radhakrishnan, S.; Rao, C.; Giljahn, L. K.; Slocumb, R. M.; Espinoza, R. E.; Khan, F.; Aird, K. G.; Beran, T.; Rubertone, J. J.; Slack, S. J.; Garcia, L.; Rousseau, D. L.; Janes, T. A; Schwartz, S. M.; Bolick, S. W.; Hurley, D. M.; Whiteside, M. A.; Miller-Gianturco, P.; Williams, M. A.; Herget, K.; Sweeney, C.; Johnson, A. T.; Cheteri, M. B. K.; Santiago, P. M.; Blankenship, S. E.; Farley, S.; Borchers, R.; Malicki, R.; Espinoza, J. R.; Grandpre, J.; Wilson, R.; Edwards, B. K.; Mariotto, A.; Lei, Y.; Wang, N.; Chen, J. S.; Zhou, Y.; He, Y. T.; Song, G. H.; Gu, X. P.; Mei, D.; Mu, H. J.; Ge, H. M.; Wu, T. H.; Li, Y. Y.; Zhao, D. L.; Jin, F.; Zhang, J. H.; Zhu, F. D.; Junhua, Q.; Yang, Y. L.; Jiang, C. X.; Biao, W.; Wang, J.; Li, Q. L.; Yi, H.; Zhou, X.; Dong, J.; Li, W.; Fu, F. X.; Liu, S. Z.; Chen, J. G.; Zhu, J.; Li, Y. H.; Lu, Y. Q.; Fan, M.; Huang, S. Q.; Guo, G. P.; Zhaolai, H.; Wei, K.; Zeng, H.; Demetriou, A. V.; Mang, W. K.; Ngan, K. C.; Kataki, A. C.; Krishnatreya, M.; Jayalekshmi, P. A.; Sebastian, P.; Nandakumar, A.; Malekzadeh, R.; Roshandel, G.; Keinan-Boker, L.; Silverman, B. G.; Ito, H.; Nakagawa, H.; Sato, M.; Tobori, F.; Nakata, I.; Teramoto, N.; Hattori, M.; Kaizaki, Y.; Moki, F.; Sugiyama, H.; Utada, M.; Nishimura, M.; Yoshida, K.; Kurosawa, K.; Nemoto, Y.; Narimatsu, H.; Sakaguchi, M.; Kanemura, S.; Naito,

M.; Narisawa, R.; Miyashiro, I.; Nakata, K.; Sato, S.; Yoshii, M.; Oki, I.; Fukushima, N.; Shibata, A.; Iwasa, K.; Ono, C.; Nimri, O.; Jung, K. W.; Won, Y. J.; Alawadhi, E.; Elbasmi, A.; Manan, A. A.; Adam, F.; Sanjaajmats, E.; Tudev, U.; Ochir, C.; Khater, A. M. A.; Mistiri, M. M. E.; Teo, Y. Y.; Chiang, C. J.; Lee, W. C.; Buasom, R.; Sangrajrang, S.; Kamsa-ard, S.; Wiangnon, S.; Daoprasert, K.; Pongnikorn, D.; Leklob, A.; Sangkitipaiboon, S.; Geater, S. L.; Sriplung, H.; Ceylan, O.; Kög, I.; Dirican, O.; Köse, T.; Gurbuz, T.; Karaşahin, F. E.; Turhan, D.; Aktaş, U.; Halat, Y.; Yakut, C. I.; Altinisik, M.; Cavusoglu, Y.; Türkköylü, A.; Üçüncü, N.; Hackl, M.; Zborovskaya, A. A.; Aleinikova, O. V.; Henau, K.; Eycken, L. V.; Valerianova, Z.; Yordanova, M. R.; Šekerija, M.; Dušek, L.; Zvolský, M.; Storm, H.; Innos, K.; Mägi, M.; Malila, N.; Seppä, K.; Jégu, J.; Velten, M.; Cornet, E.; Troussard, X.; Bouvier, A. M.; Guizard, A. V.; Bouvier, V.; Launoy, G.; Arveux, P.; Maynadié, M.; Mounier, M.; Woronoff, A. S.; Daoulas, M.; Robaszkiewicz, M.; Clavel, J.; Goujon, S.; Lacour, B.; Baldi, I.; Pouchieu, C.; Amadeo, B.; Coureau, G.; Orazio, S.; Preux, P. M.; Rharbaoui, F.; Marrer, E.; Trétarre, B.; Colonna, M.; Delafosse, P.; Ligier, K.; Plouvier, S.; Cowppli-Bony, A.; Molinié, F.; Bara, S.; Ganry, O.; Lapôtre-Ledoux, B.; Grosclaude, P.; Bossard, N.; Uhry, Z.; Bray, F.; Piñeros, M.; Stabenow, R.; Wilsdorf-Köhler, H.; Eberle, A.; Luttmann, S.; Löhden, I.; Nennecke, A. L.; Kieschke, J.; Sirri, E.; Emrich, K.; Zeissig, S. R.; Holleczek, B.; Eisemann, N.; Katalinic, A.; Asquez, R. A.; Kumar, V.; Petridou, E.; Ólafsdóttir, E. J.; Tryggvadóttir, L.; Clough-Gorr, K.; Walsh, P. M.; Sundseth, H.; Mazzoleni, G.; Vittadello, F.; Coviello, E.; Cuccaro, F.; Galasso, R.; Sampietro, G.; Giacomin, A.; Magoni, M.; Ardizzone, A.; D'Argenzio, A.; Castaing, M.; Grosso, G.; Lavecchia, A. M.; Sardo, A. S.; Gola, G.; Gatti, L.; Ricci, P.; Ferretti, S.; Serraino, D.; Zucchetto, A.; Celesia, M. V.; Filiberti, R. A.; Pannozzo, F.; Melcarne, A.; Quarta, F.; Russo, A. G.; Carrozzi, G.; Cirilli, C.; d'Oro, L. C.; Rognoni, M.; Fusco, M.; Vitale, M. F.; Usala, M.; Cusimano, R.; Mazzucco, W.; Michiara, M.; Sgargi, P.; Boschetti, L.; Borciani, E.; Seghini, P.; Maule, M. M.; Merletti, F.; Tumino, R.; Mancuso, P.; Vicentini, M.; Cassetti, T.; Sassatelli, R.; Falcini, F.; Giorgetti, S.; Caiazzo, A. L.; Cavallo, R.; Cesaraccio, R.; Pirino, D. R.; Contrino, M. L.; Tisano, F.; Fanetti, A. C.; Maspero, S.; Carone, S.; Mincuzzi, A.; Candela, G.; Scuderi, T.; Gentilini, M. A.; Piffer, S.; Rosso, S.; Barchielli, A.; Caldarella, A.; Bianconi, F.; Stracci, F.; Contiero, P.; Tagliabue, G.; Rugge, M.; Zorzi, M.; Beggiato, S.; Brustolin, A.; Berrino, F.; Gatta, G.; Sant, M.; Buzzoni, C.; Mangone, L.; Capocaccia, R.; Angelis, R. D.; Zanetti, R.; Maurina, A.; Pildava, S.; Lipunova, N.; Vincerževskienė, I.; Agius, D.; Calleja, N.; Siesling, S.; Larønningen, S.; Møller, B.; Dyzmann-Sroka, A.; Trojanowski, M.; Góźdź, S.; Mężyk, R.; Mierzwa, T.; Molong, L.; Rachtan, J.; Szewczyk, S.; Błaszczyk, J.; Kępska, K.; Kościańska, B.; Tarocińska, K.; Zwierko, M.; Drosik, K.; Maksimowicz, K. M.; Purwin-Porowska, E.; Reca, E.; Wójcik-Tomaszewska, J.; Tukiendorf, A.; Grądalska-Lampart, M.; Radziszewska, A. U.; Gos, A.; Talerczyk, M.; Wyborska, M.; Didkowska, J. A.; Wojciechowska, U.; Bielska-Lasota, M.; de Lacerda G. F. Rego, R. A.; Bastos, J.; Silva, M. A.; Antunes, L.; Pontes, J. L.; Mayer-da-Silva, A.; Miranda, A.; Blaga, L. M.; Coza, D.; Gusenkova, L.; Lazarevich, O.; Prudnikova, O.; Vjushkov, D. M.; Egorova, A. G.; Orlov, A. E.; Kudyakov, L. A.; Pikalova, L. V.; Adamcik, J.; Diba, C. S.; Primic-Žakelj, M.; Zadnik, V; Larrañaga, N.; de Munain, A. L.; Herrera, A. A.; Redondas, R.; Marcos-Gragera, R.; Gil, M. L. V.; Molina, E.; Perez, M. J. S.; Sureda, P. F.; Montserrat, M. R.; Chirlaque, M. D.; Navarro, C.; Ardanaz, E. E.; Guevara, M. M.; Fernández-Delgado, R.; Peris-Bonet, R.; Carulla, M.; Galceran, J.; Alberich, C.; Vicente-Raneda, M.; Khan, S.; Pettersson, D.; Dickman, P.; Avelina, I.; Staehelin, K.; Camey, B.; Bouchardy, C.; Schaffar, R.; Frick, H.; Herrmann, C.; Bulliard, J. L.; Maspoli-Conconi, M.; Kuehni, C. E.; Redmond, S. M.; Bordoni, A.; Ortelli, L.; Chiolero, A.; Konzelmann, I.; Matthes, K. L.; Rohrmann, S.; Broggio, J.; Rashbass, J.; Fitzpatrick, D.; Gavin, A.; Clark, D. I.; Deas, A. J.; Huws, D. W.; White, C.; Montel, L.; Rachet, B.; Turculet, A. D.; Stephens, R.; Chalker, E.; Phung, H.; Walton, R.; You, H.; Guthridge, S.; Johnson, F.; Gordon, P.; D'Onise, K.; Priest, K.; Stokes, B. C.; Venn, A.; Farrugia, H.; Thursfield, V.; Dowling, J.; Currow, D.; Hendrix, J.; Lewis, C. Global Surveillance of Trends in Cancer Survival 2000−14 (CONCORD-3): Analysis of Individual Records for 37 513 025 Patients Diagnosed with One of 18 Cancers from 322 Population-Based Registries in 71 Countries. *Lancet* **2018**, *391* (10125), 1023–1075.

(9) Chari, S. T.; Kelly, K.; Hollingsworth, M. A.; Thayer, S. P.; Ahlquist, D. A.; Andersen, D. K.; Batra, S. K.; Brentnall, T. A.; Canto, M.; Cleeter, D. F.; Firpo, M. A.; Gambhir, S. S.; Go, V. L. W.; Hines, O. J.; Kenner, B. J.; Klimstra, D. S.; Lerch, M. M.; Levy, M. J.; Maitra, A.; Mulvihill, S. J.; Petersen, G. M.; Rhim, A. D.; Simeone, D. M.; Srivastava, S.; Tanaka, M.; Vinik, A. I.; Wong, D. Early Detection of Sporadic Pancreatic Cancer: Summative Review. *Pancreas* **2015**, *44* (5), 693.

(10) Poh, A. R.; Ernst, M. Tumor-Associated Macrophages in Pancreatic Ductal Adenocarcinoma: Therapeutic Opportunities and Clinical Challenges. *Cancers* **2021**, *13* (12), No. 2860.

(11) Yu, M.; Guan, R.; Hong, W.; Zhou, Y.; Lin, Y.; Jin, H.; Hou, B.; Jian, Z. Prognostic Value of Tumor-Associated Macrophages in Pancreatic Cancer: A Meta-Analysis. *Cancer Manag. Res.* **2019**, *11*, 4041–4058.

(12) Liermann, J.; Munter, M.; Naumann, P.; Abdollahi, A.; Krempien, R.; Debus, J. Cetuximab, Gemcitabine and Radiotherapy in Locally Advanced Pancreatic Cancer: Long-Term Results of the Randomized Controlled Phase II PARC Trial. *Clin. Transl. Radiat. Oncol.* **2022**, *34*, 15–22.

(13) Butterworth, K. T.; McMahon, S. J.; Taggart, L. E.; Prise, K. M. Radiosensitization by Gold Nanoparticles: Effective at Megavoltage Energies and Potential Role of Oxidative Stress. *Transl. Cancer Res.* **2013**, *2* (4), 269–279.

(14) Penninckx, S.; Heuskin, A.-C.; Michiels, C.; Lucas, S. The Role of Thioredoxin Reductase in Gold Nanoparticle Radiosensitization Effects. *Nanomedicine* **2018**, *13* (22), 2917–2937.

(15) Li, S.; Penninckx, S.; Karmani, L.; Heuskin, A.-C.; Watillon, K.; Marega, R.; Zola, J.; Corvaglia, V.; Genard, G.; Gallez, B.; Feron, O.; Martinive, P.; Bonifazi, D.; Michiels, C.; Lucas, S. LET-Dependent Radiosensitization Effects of Gold Nanoparticles for Proton Irradiation. *Nanotechnology* **2016**, *27* (45), No. 455101.

(16) Genard, G.; Wera, A.-C.; Huart, C.; Le Calve, B.; Penninckx, S.; Fattaccioli, A.; Tabarrant, T.; Demazy, C.; Ninane, N.; Heuskin, A.-C.; Lucas, S.; Michiels, C. Proton Irradiation Orchestrates Macrophage Reprogramming through NFκB Signaling. *Cell Death Dis.* **2018**, *9* (7), 1–13.

(17) Kim, S.; Choe, J. H.; Lee, G. J.; Kim, Y. S.; Kim, S. Y.; Lee, H.-M.; Jin, H. S.; Kim, T. S.; Kim, J.-M.; Cho, M.-J.; Shin, E.-C.; Jo, E.-K.; Kim, J.-S. Ionizing Radiation Induces Innate Immune Responses in Macrophages by Generation of Mitochondrial Reactive Oxygen Species. *Radiat. Res.* **2016**, *187* (1), 32–41.

(18) Griess, B.; Mir, S.; Datta, K.; Teoh-Fitzgerald, M. Scavenging Reactive Oxygen Species Selectively Inhibits M2 Macrophage Polarization and Their Pro-Tumorigenic Function in Part, via Stat3 Suppression. *Free Radic. Biol. Med.* **2020**, *147*, 48–60.

(19) Meng, Y.; Beckett, M. A.; Liang, H.; Mauceri, H. J.; van Rooijen, N.; Cohen, K. S.; Weichselbaum, R. R. Blockade of Tumor Necrosis Factor α Signaling in Tumor-Associated Macrophages as a Radiosensitizing Strategy. *Cancer Res.* **2010**, *70* (4), 1534–1543.

(20) Klug, F.; Prakash, H.; Huber, P. E.; Seibel, T.; Bender, N.; Halama, N.; Pfirschke, C.; Voss, R. H.; Timke, C.; Umansky, L.; Klapproth, K.; Schäkel, K.; Garbi, N.; Jäger, D.; Weitz, J.; Schmitz-Winnenthal, H.; Hämmerling, G. J.; Beckhove, P. Low-Dose Irradiation Programs Macrophage Differentiation to an iNOS+/M1 Phenotype That Orchestrates Effective T Cell Immunotherapy. *Cancer cell* **2013**, *24* (5), 589–602.

(21) Ni, J.; Guo, T.; Zhou, Y.; Jiang, S.; Zhang, L.; Zhu, Z. STING Signaling Activation Modulates Macrophage Polarization via CCL2 in Radiation-Induced Lung Injury. *J. Transl. Med.* **2023**, *21* (1), No. 590.

(22) Beach, C.; MacLean, D.; Majorova, D.; Arnold, J. N.; Olcina, M. M. The Effects of Radiation Therapy on the Macrophage Response in Cancer. *Front. Oncol.* **2022**, *12*.

https://doi.org/10.1021/acsabm.6c00342
ACS Appl. Bio Mater. XXXX, XXX, XXX–XXX

(23) Wu, Q.; Allouch, A.; Martins, I.; Modjtahedi, N.; Deutsch, E.; Perfettini, J.-L. Macrophage Biology Plays a Central Role during Ionizing Radiation-Elicited Tumor Response. *Biomed. J.* **2017**, *40* (4), 200–211.
(24) Kurakula, M.; Rao, G. S. N. K. Pharmaceutical Assessment of Polyvinylpyrrolidone (PVP): As Excipient from Conventional to Controlled Delivery Systems with a Spotlight on COVID-19 Inhibition. *J. Drug Deliv. Sci. Technol.* **2020**, *60*, No. 102046.
(25) Ibrahim, M.; Ramadan, E.; Elsadek, N. E.; Emam, S. E.; Shimizu, T.; Ando, H.; Ishima, Y.; Elgarhy, O. H.; Sarhan, H. A.; Hussein, A. K.; Ishida, T. Polyethylene Glycol (PEG): The Nature, Immunogenicity, and Role in the Hypersensitivity of PEGylated Products. *J. Control. Release* **2022**, *351*, 215–230.
(26) Baganizi, D. R.; Nyairo, E.; Duncan, S. A.; Singh, S R; Dennis, V. A. Interleukin-10 Conjugation to Carboxylated PVP-Coated Silver Nanoparticles for Improved Stability and Therapeutic Efficacy. *Nanomaterials* **2017**, *7* (7), No. 165.
(27) Sivaraman, S. K.; Kumar, S.; Santhanam, V. Monodisperse Sub-10nm Gold Nanoparticles by Reversing the Order of Addition in Turkevich Method − The Role of Chloroauric Acid. *J. Colloid Interface Sci.* **2011**, *361* (2), 543–547.
(28) George, E.; Goswami, A.; Lodhiya, T.; Padwal, P.; Iyer, S.; Gauttam, I.; Sethi, L.; Jeyasankar, S.; Sharma, P. R.; Dravid, A. A.; Mukherjee, R.; Agarwal, R. Immunomodulatory Effect of Mycobacterial Outer Membrane Vesicles Coated Nanoparticles. *Biomater. Adv.* **2022**, *139*, No. 213003.
(29) Wéra, A.-C.; Riquier, H.; Heuskin, A.-C.; Michiels, C.; Lucas, S. In Vitro Irradiation Station for Broad Beam Radiobiological Experiments. *Nucl. Instrum. Methods Phys. Res., Sect. B.* **2011**, *269* (24), 3120–3124.
(30) Ziegler, J. F.; Ziegler, M. D.; Biersack, J. P. SRIM − The Stopping and Range of Ions in Matter (2010). *Nucl. Instrum. Methods Phys. Res. B.* **2010**, *268* (11), 1818–1823.
(31) Turkevich, J.; Stevenson, P. C.; Hillier, J. A Study of the Nucleation and Growth Processes in the Synthesis of Colloidal Gold. *Discuss. Faraday Soc.* **1951**, *11* (0), 55–75.
(32) Chithrani, B. D.; Chan, W. C. W. Elucidating the Mechanism of Cellular Uptake and Removal of Protein-Coated Gold Nanoparticles of Different Sizes and Shapes. *Nano Lett.* **2007**, *7* (6), 1542–1550.
(33) Chithrani, B. D.; Ghazani, A. A.; Chan, W. C. W. Determining the Size and Shape Dependence of Gold Nanoparticle Uptake into Mammalian Cells. *Nano Lett.* **2006**, *6* (4), 662–668.
(34) Penninckx, S.; Heuskin, A.-C.; Michiels, C.; Lucas, S. Thioredoxin Reductase Activity Predicts Gold Nanoparticle Radiosensitization Effect. *Nanomaterials* **2019**, *9* (2), No. 295.
(35) Häkkinen, H. The Gold−Sulfur Interface at the Nanoscale. *Nat. Chem.* **2012**, *4* (6), 443–455.
(36) Mdluli, P. S.; Sosibo, N. M.; Revaprasadu, N.; Karamanis, P.; Leszczynski, J. Surface Enhanced Raman Spectroscopy (SERS) and Density Functional Theory (DFT) Study for Understanding the Regioselective Adsorption of Pyrrolidinone on the Surface of Silver and Gold Colloids. *J. Mol. Struct.* **2009**, *935* (1), 32–38.
(37) PVP encapsulated Au nanoparticles. *ChemTube3D*. https://www.chemtube3d.com/aunano_pvp-encapsulated-au-nanoparticles/ (accessed May 06,2025).
(38) Omping, J.; Unabia, R.; Reazo, R. L.; Lapening, M.; Lumod, R.; Ruda, A.; Rivera, R. B.; Sayson, N. L.; Latayada, F.; Capangpangan, R.; Dumancas, G.; Malaluan, R.; Lubguban, A.; Petalcorin, G.Jr.; Alguno, A. Facile Synthesis of PEGylated Gold Nanoparticles for Enhanced Colorimetric Detection of Histamine. *ACS Omega* **2024**, *9* (12), 14269–14278.
(39) Jain, P. K.; El-Sayed, I. H.; El-Sayed, M. A. Au Nanoparticles Target Cancer. *Nano Today* **2007**, *2* (1), 18–29.
(40) Cruje, C.; Yang, C.; Uertz, J.; van Prooijen, M.; Chithrani, B. D. Optimization of PEG Coated Nanoscale Gold Particles for Enhanced Radiation Therapy. *RSC Adv.* **2015**, *5* (123), No. 101525.
(41) Liu, L.; Yu, W.; Seitsonen, J.; Xu, W.; Lehto, V.-P. Correct Identification of the Core-Shell Structure of Cell Membrane-Coated Polymeric Nanoparticles. *Chem. - Eur. J.* **2022**, *28* (68), No. e202200947.
(42) Shi, L.; Zhang, J.; Zhao, M.; Tang, S.; Cheng, X.; Zhang, W.; Li, W.; Liu, X.; Peng, H.; Wang, Q. Effects of Polyethylene Glycol on the Surface of Nanoparticles for Targeted Drug Delivery. *Nanoscale* **2021**, *13* (24), 10748–10764.
(43) Kah, J. C. Y.; Wong, K. Y.; Neoh, K. G.; Song, J. H.; Fu, J. W. P.; Mhaisalkar, S.; Olivo, M.; Sheppard, C. J. R. Critical Parameters in the Pegylation of Gold Nanoshells for Biomedical Applications: An in Vitro Macrophage Study. *J. Drug Target.* **2009**, *17* (3), 181–193.
(44) Walkey, C. D.; Olsen, J. B.; Guo, H.; Emili, A.; Chan, W. C. W. Nanoparticle Size and Surface Chemistry Determine Serum Protein Adsorption and Macrophage Uptake. *J. Am. Chem. Soc.* **2012**, *134* (4), 2139–2147.
(45) Gaucher, G.; Asahina, K.; Wang, J.; Leroux, J.-C. Effect of Poly(N-Vinyl-Pyrrolidone)-Block-Poly(d,l-Lactide) as Coating Agent on the Opsonization, Phagocytosis, and Pharmacokinetics of Biodegradable Nanoparticles. *Biomacromolecules* **2009**, *10* (2), 408–416.
(46) Mohamed, T.; Matou-Nasri, S.; Farooq, A.; Whitehead, D.; Azzawi, M. Polyvinylpyrrolidone-Coated Gold Nanoparticles Inhibit Endothelial Cell Viability, Proliferation, and ERK1/2 Phosphorylation and Reduce the Magnitude of Endothelial-Independent Dilator Responses in Isolated Aortic Vessels. *Int. J. Nanomed.* **2017**, *12*, 8813–8830.
(47) Gustafson, H. H.; Holt-Casper, D.; Grainger, D. W.; Ghandehari, H. Nanoparticle Uptake: The Phagocyte Problem. *Nano Today* **2015**, *10* (4), 487–510.
(48) Becherini, C.; Lancia, A.; Detti, B.; Lucidi, S.; Scartoni, D.; Ingrosso, G.; Carnevale, M. G.; Roghi, M.; Bertini, N.; Orsatti, C.; Mangoni, M.; Francolini, G.; Marani, S.; Giacomelli, I.; Loi, M.; Pergolizzi, S.; Bonzano, E.; Aristei, C.; Livi, L. Modulation of Tumor-Associated Macrophage Activity with Radiation Therapy: A Systematic Review. *Strahlenther. Onkol.* **2023**, *199* (12), 1173–1190.
(49) Genard, G.; Lucas, S.; Michiels, C. Reprogramming of Tumor-Associated Macrophages with Anticancer Therapies: Radiotherapy versus Chemo- and Immunotherapies. *Front. Immunol.* **2017**, *8*.
(50) Birben, E.; Sahiner, U. M.; Sackesen, C.; Erzurum, S.; Kalayci, O. Oxidative Stress and Antioxidant Defense. *World Allergy Organ. J.* **2012**, *5* (1), 9–19.
(51) Rendra, E.; Riabov, V.; Mossel, D. M.; Sevastyanova, T.; Harmsen, M. C.; Kzhyshkowska, J. Reactive Oxygen Species (ROS) in Macrophage Activation and Function in Diabetes. *Immunobiology* **2019**, *224* (2), 242–253.
(52) Tan, H.-Y.; Wang, N.; Li, S.; Hong, M.; Wang, X.; Feng, Y. The Reactive Oxygen Species in Macrophage Polarization: Reflecting Its Dual Role in Progression and Treatment of Human Diseases. *Oxid. Med. Cell. Longev.* **2016**, *2016*, No. e2795090.
(53) Daems, N.; Penninckx, S.; Nelissen, I.; Van Hoecke, K.; Cardinaels, T.; Baatout, S.; Michiels, C.; Lucas, S.; Aerts, A. Gold Nanoparticles Affect the Antioxidant Status in Selected Normal Human Cells. *Int. J. Nanomed.* **2019**, *14*, 4991–5015.
(54) Hingorani, S R; Wang, L.; Multani, A. S.; Combs, C.; Deramaudt, T. B.; Hruban, R. H.; Rustgi, A. K.; Chang, S.; Tuveson, D. A. Trp53R172H and KrasG12D Cooperate to Promote Chromosomal Instability and Widely Metastatic Pancreatic Ductal Adenocarcinoma in Mice. *Cancer Cell* **2005**, *7* (5), 469–483.
(55) Xing, Q.; Feng, Y.; Sun, H.; Yang, S.; Sun, T.; Guo, X.; Ji, F.; Wu, B.; Zhou, D. Scavenger Receptor MARCO Contributes to Macrophage Phagocytosis and Clearance of Tumor Cells. *Exp. Cell Res.* **2021**, *408* (2), No. 112862.
(56) Lunov, O.; Syrovets, T.; Loos, C.; Beil, J.; Delacher, M.; Tron, K.; Nienhaus, G. U.; Musyanovych, A.; Mailänder, V.; Landfester, K.; Simmet, T. Differential Uptake of Functionalized Polystyrene Nanoparticles by Human Macrophages and a Monocytic Cell Line. *ACS Nano* **2011**, *5* (3), 1657–1669.

https://doi.org/10.1021/acsabm.6c00342
ACS Appl. Bio Mater. XXXX, XXX, XXX–XXX